AGU PUBLICATIONS

Geophysical Research Letters

RESEARCH LETTER
10.1002/2016GL069591

Key Points:
- The MARSIS radar revealed pulse-created, crust magnetic field-aligned plasma bubbles in the Mars ionosphere
- Ducted wave signatures occur infrequently owing to the ionospheric plasma distribution
- Ducted waves show the cutoff frequencies higher than the theoretical upper hybrid frequency

Supporting Information:
- Supporting Information S1

Correspondence to:
Z. Zhang,
zfzhang@cug.edu.cn

Citation:
Zhang, Z., R. Orosei, Q. Huang, and J. Zhang (2016), Ducted electromagnetic waves in the Martian ionosphere detected by the Mars Advanced Radar for Subsurface and Ionosphere Sounding radar, *Geophys. Res. Lett.*, *43*, 7381–7388, doi:10.1002/2016GL069591.

Received 14 MAY 2016
Accepted 11 JUL 2016
Accepted article online 14 JUL 2016
Published online 30 JUL 2016

Ducted electromagnetic waves in the Martian ionosphere detected by the Mars Advanced Radar for Subsurface and Ionosphere Sounding radar

Zhenfei Zhang[1], Roberto Orosei[2], Qian Huang[3], and Jie Zhang[1]

[1]Institute of Mathematical Geology and Remote Sensing, China University of Geosciences, Wuhan, China, [2]Istituto di Radioastronomia, Istituto Nazionale di Astrofisica, Via Piero Gobetti, Bologna, Italy, [3]Institute of Planetary Science, China University of Geosciences, Wuhan, China

Abstract In the data of the Mars Advanced Radar for Subsurface and Ionosphere Sounding on board the European Space Agency (ESA) mission Mars Express (MEX), a distinctive type of signals (called the "epsilon signature"), which is similar to that previously detected during radio sounding of the terrestrial *F* region ionosphere, is found. The signature is interpreted to originate from multiple reflections of electromagnetic waves propagating along sounder pulse-created, crustal magnetic field-aligned plasma bubbles (waveguides). The signatures have a low (below 0.5%) occurrence rate and apparent cutoff frequencies 3–5 times higher than the theoretical one for an ordinary mode wave. These properties are explained by the influence of the perpendicular ionospheric plasma density gradient and the sounder pulse frequency on the formation of waveguides.

1. Introduction

The main body of the dayside Martian ionosphere (M2 layer) is basically a Chapman layer. Its electron density peaks at an altitude of approximately 130 km at intermediate solar zenith angles (SZAs) and decreases upward with a scale height of a few tens of kilometers [*Gurnett et al*., 2005; *Fox and Yeager*, 2006; *Nielsen et al*., 2006; *Gurnett et al*., 2008; *Morgan et al*., 2008; *Withers*, 2009; *Němec et al*., 2011]. However, this morphology is strongly modified if crustal magnetic anomalies develop [*Acuña et al*., 1998, 2001; *Andrews et al*., 2013, 2015; *Langlais et al*., 2004; *Lillis et al*., 2008]. The field lines may control the ionospheric plasma motion to form local structures. The closed field lines may produce plasma cylinders, which may extend to several hundred kilometers in the horizontal directions and can be detected at altitudes above 400 km [*Ness et al*., 2000; *Mitchell et al*., 2001; *Krymskii et al*., 2002; *Duru et al*., 2006]. Where the field lines are vertical, the electron density and density scale height of the ionosphere may increase to form plasma bulges because of solar wind energetic particles input along the open field lines [*Mitchell et al*., 2001; *Krymskii et al*., 2002; *Nielsen et al*., 2007; *Gurnett et al*., 2008]. In the downstream regions of the magnetic anomalies, plasma flux ropes with diameters of several hundred kilometers may form because of solar wind stretching and shearing of the crustal fields [*Morgan et al*., 2011; *Beharrell and Wild*, 2012].

As the crustal magnetic fields modify the ionosphere morphology, ionospheric plasma must have been magnetized to some extent. Therefore, during radio sounding of the ionosphere, anisotropic dielectric properties associated with the magnetization could be observed. To verify this anticipation, we examined the data of the Mars Advanced Radar for Subsurface and Ionosphere Sounding (MARSIS) on board the European Space Agency (ESA) mission Mars Express (MEX) [*Picardi et al*., 2004; *Gurnett et al*., 2005]. The MARSIS data and technique have been described by several authors [e.g., *Picardi et al*., 2004; *Gurnett et al*., 2005; *Morgan et al*., 2008; *Jordan et al*., 2009; *Duru et al*., 2010; *Morgan et al*., 2013; *Zhang et al*., 2015]. A MARSIS measurement (called the frame) can be visualized using an ionogram (i.e., a plot of the echo intensity as a function of the time delay and frequency). To date, the data acquired from June 2005 to October 2013 have been made publicly available, including a total of approximately 120,200 frames on 7700 MEX orbits. Four types of the MARSIS signals were utilized to retrieve information about the ionosphere: (1) Vertical echoes (those from the nadir direction) were used to reconstruct the vertical ionospheric density profiles [e.g., *Nielsen et al*., 2006; *Gurnett et al*., 2008; *Morgan et al*., 2008, 2013], constrain peak density variations [*Wang et al*., 2012], or characterize sublayers inside the main layer [e.g., *Kopf et al*., 2008; *Zhang et al*., 2015]. (2) Oblique echoes (those from the off-nadir regions) were used to register plasma bulges [e.g., *Gurnett et al*., 2005; *Nielsen et al*., 2007; *Andrews et al*., 2014;

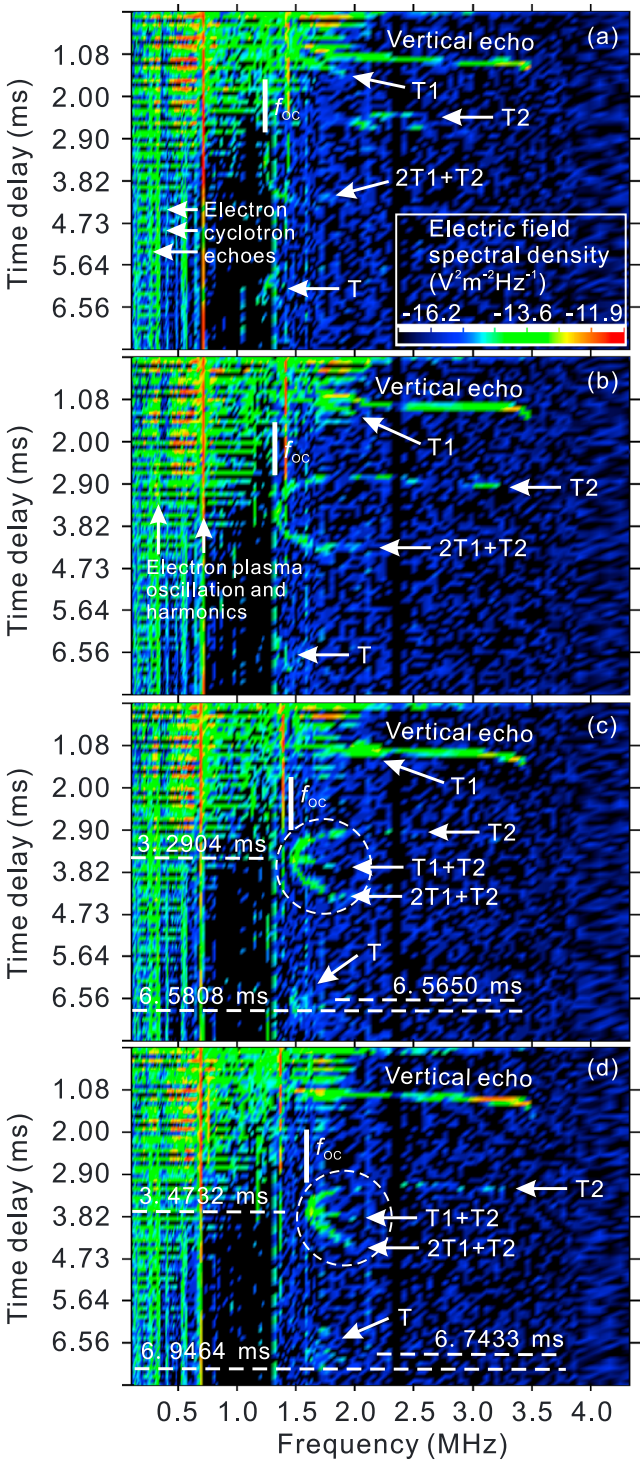

Figure 1. Examples of the MARSIS frames wherein the epsilon signatures are seen. (a–d) The ionograms for orbit 2359, frames 158–161 (acquisition time stamps: 2005-318 T06:17:13.437–2005-318 T06:17: 36.066). The circles highlight the epsilon signatures that are most clearly seen. The vertical bars indicate the observed cutoff frequencies (f_{OC}) (the leftmost edges) of the epsilon signatures. The dashed line in Figures 1c and 1d indicate that trace T has a time delay shorter (by <3%) than twice that of the epsilon signature. The logarithm of the electric field density is color coded in the same manner for all the four panels.

Diéval et al., 2015] and characterize the horizontal density gradient near the terminator [*Duru et al.*, 2010]. (3) Electron plasma oscillation harmonic echoes were used to estimate the in situ electron plasma frequency [e.g., *Gurnett et al.*, 2008; *Duru et al.*, 2008; *Gurnett et al.*, 2010]. (4) Electron cyclotron echoes were exploited to measure the in situ magnetic field magnitude [e.g., *Gurnett et al.*, 2008; *Akalin et al.*, 2010; *Morgan et al.*, 2011]. In this paper, we report a new type of MARSIS echoes, which can be interpreted to indicate anisotropic dielectric properties of the ionosphere, associated with the crustal magnetic fields, and the formation of density irregularities by the MARSIS sounder pulses. We will describe the characteristics of the signals in section 2 and discuss their origin and implications in section 3.

2. Phenomena

Figure 1 shows the four successive ionograms (frames 158–161) on the MEX orbit no. 2359. In the middle parts of the individual ionograms, a "fixed" combination of several oblique echo traces can be seen (highlighted using the circles in Figures 1c and 1d). We call this feature the "epsilon signature" following *Dyson and Benson* [1978] and *Benson* [1997] who described similar features found in the terrestrial *F* region ionosphere in the data of International Satellites for Ionospheric Studies (ISIS) [see *Benson*, 1997, Figures 1 and 2]. In Figure 1, the echo traces associated with the epsilon signature are specifically labeled for ease of reference. The upper, middle, and lower branches of the signature are labeled as "T2," "T1 + T2," and "2 T1 + T2," respectively. Above the signature, an oblique echo is labeled as "T1," which is near the vertical echo trace or overlaps it.

Table 1. MARSIS AIS Frames With Distinguishable Epsilon Signatures

Orbit No. (Frm No.) [a]	Acquisition Time[b]	Latitude (deg)	E. Longitude (deg)	SZA[c] (deg)	z_{SC}[d] (km)	f_{OC}[e] (MHz)	f_{ce}[f] (kHz)	f_p[g] (MHz)
2073 (136–139)	2005-238 T04:52:36.275	−9.514	169.567	44.73	292.18	1.3453	3.647	0.3719
2359 (158–163)	2005-318 T06:17:13.437	−48.714	190.888	36.57	287.25	1.2138	5.470	0.3828
3286 (141–148)	2006-212 T18:52:01.842	32.686	13.544	25.21	336.27	1.2578	1.094	0.3824
4238 (153–156)	2007-114 T09:03:46.934	−31.629	158.031	48.89	298.39	1.1485	2.188	0.2846
6665 (52–60)	2009-071 T17:51:45.860	−66.603	194.678	48.83	442.68	1.2138	1.563	0.3499
7286 (172–176)	2009-250 T03:26:11.007	13.648	338.931	62.50	348.42	1.2796	1.2157	0.4375
7418 58–67	2009-288 T01:38:49.937	32.973	330.569	49.03	375.61	1.1702	3.647	0.2841

[a]Orbit number with the frame serial numbers in parentheses. All the data listed pertain to the first frame of the frame group.
[b]Time stamp of the observation in the data file.
[c]Solar zenith angle.
[d]Spacecraft altitude.
[e]Lowest frequency of the epsilon signature (the observed cutoff frequency).
[f]In situ electron cyclotron frequency, estimated using the method by *Gurnett et al*. [2008] and *Akalin et al*. [2010], that is, f_{ce} equals the reciprocal of the time delay difference between two adjacent electron cyclotron echoes.
[g]In situ plasma frequency, estimated using the method by *Gurnett et al*. [2008] and *Duru et al*. [2006, 2008], that is, f_p equals the frequency difference between two adjacent electron plasma oscillation harmonic echoes.

Below the signature, a diffuse echo trace is labeled as "T." The lowest frequency (the left edge) of the epsilon signature is labeled as "f_{OC}" and is called the "observed cutoff frequency." In all these labels, letter T means "Trace."

The epsilon signature is composed of multiple oblique echoes and differs from the "hook structure" discovered by *Wang et al*. [2009], which characterizes deformed vertical echoes from the ionospheric topside where sublayers exist.

The epsilon signature occurs infrequently. We visually (aided by a routine, which displayed consecutive ionograms as animations of the controllable speed and facilitated the manual selection of ionograms) examined all the MARSIS active ionosphere sounding (AIS) data acquired before October 2013 and found that the epsilon signatures were distinguishable only in 46 frames on seven MEX orbits, as listed in Table 1. "Distinguishable" means that at least two of the three branches can be seen in several consecutive frames. Except for those shown in Figure 1, examples of the ionograms listed in Table 1 are displayed in the online supporting information section (four ionograms per orbit).

Besides their conspicuous shapes, the signatures also show the following characteristics. (1) They are accompanied by electron cyclotron echoes, indicating that they occur in regions where magnetic fields are strong (39–195 nT, calculated using the method of *Gurnett et al*. [2008] and *Akalin et al*. [2010], based on Table 1). (2) They mostly (80.4%) occur when the spacecraft altitude is relatively low (<400 km). (3) They mostly occur (89.1%) when the SZA is relatively low (<50°). (4) Echo trace T (about 63%) appears often but is diffuse and quite obscure. The time delay of T is shorter (by 3–13%) than twice that of the leftmost (lowest frequency) part of the epsilon signature. For example, the time delays are indicated using the dashed lines in Figures 1c and 1d. (5) The values of f_{OC} are more than 3 times higher than the in situ plasma frequency.

3. Interpretation and Discussions

3.1. Origin of the Epsilon Signature

The origin of the epsilon signatures observed in the terrestrial *F* region ionosphere using the ISIS radar was explained by *Dyson and Benson* [1978] and *Benson* [1997] as follows. The sounder pulse would generate an elongated region of plasma depletion (plasma bubble, where the electron density was reduced by a few percent [*Calvert*, 1995; *Benson*, 1997; *Gurevich et al*., 2002]), along the Earth's dipole magnetic field between the two hemispheres by the ponderomotive force. The bubble served as a waveguide, along which the wave propagated in the two opposite directions. The two waves experienced multiple reflections from the two ends of the bubble to the sensor, producing the epsilon signature. The generation of the waveguide required $f_p/|f_{ce}| \cong n$ with $f_p > |f_{ce}|$, where f_p and f_{ce} are the in situ plasma frequency and the electron cyclotron frequency, respectively, and n is an integer approximately equal to 5 [*Benson*, 1997, and references therein].

We suggest a similar explanation for the epsilon signatures shown in Figure 1 based on their similar shapes to those described by *Benson* [1997]. As illustrated in Figure 2, we consider two plasma bulges to be associated

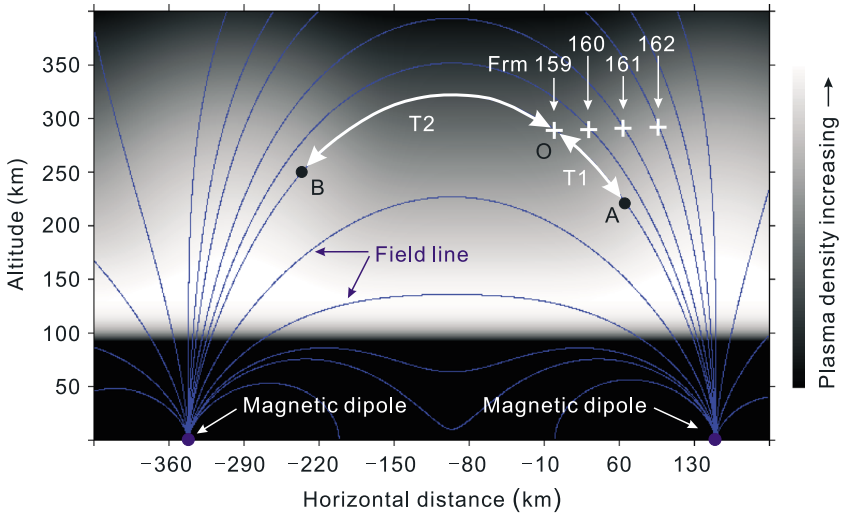

Figure 2. Schematics illustrating a possible origin of the epsilon signatures shown in Figure 1. The crosses indicate the relative positions of the spacecraft; A and B are possible reflection points; the two-headed arrows indicate the wave paths along the same field line. Paths O → A → O and O → B → O are labeled using T1 and T2 to indicate that the waves propagating along these paths are responsible for echo traces T1 and T2 in Figure 1, respectively.

with two magnetic dipoles situated on the planet surface a few hundred kilometers apart. The two dipoles are assumed to have opposite orientations; thus, the closed field lines link the two bulges. The MARSIS is assumed to be somewhere between the two bulges (point O in Figure 2). When a pulse is transmitted, it can generate a field-aligned plasma bubble, which can serve as a waveguide. Along the waveguide, the wave propagates in the opposite directions from spacecraft position O and is reflected at the positions (A and B) where the plasma frequency equals the wave frequency. The wave passing O → A → O may produce echo trace T1, and the wave passing O → B → O may produce T2. The two waves can complete the round trip path between A and B (O → A → O → B → O and O → B → O → A → O) within the same time delay, producing trace T1 + T2. The waves may continue to propagate and reflect, producing 2 T1 + T2 and T1 + 2 T2. As the sounding frequency is increased, reflection points A and B become more distant such that T2 and 2 T1 + T2 traces separate in time delay. Echo trace T is a repetition of the epsilon signature due to multiple reflections of the waves. T is obscure because the waves experience greater attenuation. The time delay of T is shorter than twice that of the signature because the waves propagate faster along an existing waveguide. The signature tends to occur when the spacecraft altitude is relatively low because at high altitudes, the crustal magnetic field is weak; thus, field-aligned waveguides cannot form. The signature tends to occur at relatively small SZAs, maybe because at large SZAs, the field lines are more probable to go to the night side, where plasma is generally thin and the waves cannot reflect.

The interpretation above stresses that multiple reflections of the electromagnetic waves propagating along a field-aligned waveguide result in the epsilon signature. It is also possible that the closed field lines were from only one dipole. In this case, one of the two ends of the waveguide approaches the normal ionospheric plasma density peak, while another end approaches a bulge.

Figure 3 shows the geographical distributions of the epsilon signatures and the crustal magnetic fields (the radial component), whereby we see that the signatures tend to occur near the field intensity peaks and near the regions where the radial components of the fields change sign, confirming the interpretation presented in Figure 2. The geographic locations of the signatures are also close to the locations of the relative concentration of the isotropic electron pitch angle distributions (PADs) [see *Brain et al*., 2007, Figure 11a]. These types of PADs were assumed to indicate electrons trapped by the closed magnetic field lines [*Brain et al*., 2007]. This also indicates that the epsilon signatures are related to the crustal magnetic fields.

In brief, most of the observed phenomena described in section 2 can be explained by introducing a field-aligned waveguide as depicted in Figure 2. In section 3.2, we discuss why the epsilon signature occurs infrequently and why its observed cutoff frequency is much higher than the in situ plasma frequency. The answers to these questions involve the formation of a waveguide.

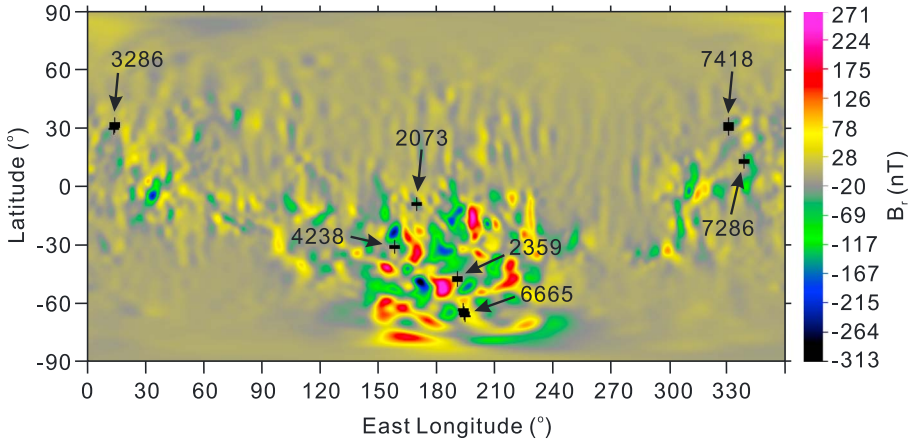

Figure 3. Geographical positions (black crosses) of the epsilon signatures. The numbers indicate the MEX orbit numbers listed in Table 1. The background is the modeled radial component of the crustal magnetic field (B_r) at an altitude of 200 km (B. Langlais, personal communication, 2016).

3.2. Infrequency of the Epsilon Signature Occurrence and Waveguide Formation

About 10,000 MARSIS frames made at spacecraft altitudes below 400 km and SZA < 60° exhibit electron cyclotron echoes. The number of epsilon signatures is 46 (Table 1), giving a low occurrence rate below 0.5%. This low occurrence rate may be explained as follows.

According to the cold plasma ray tracing theory [*Fitzpatrick*, 2008], in the three-dimensional space, an ordinary mode (O mode) wave, which propagates independently of magnetic fields, satisfies

$$\frac{d\mathbf{k}}{dt} = -\frac{e^2}{2\varepsilon_0 m_e \omega}\nabla N, \tag{1}$$

where t is the time, $\mathbf{k}$ is the wave vector, $\omega = 2\pi f$ is the angular frequency of the wave, e is the electron charge, m_e is the electron mass, ε_0 is the vacuum permittivity, and N is the plasma density. Equation (1) states that the wave vector tends to be deflected to the direction opposite to the plasma density gradient or to the direction of the refractive index (n) increase ($n^2 = 1 - \omega_p^2/\omega^2$, where ω_p is the angular plasma frequency). The plasma density in the Martian ionosphere has a general trend to decrease upward from the density peak [e.g., *Gurnett et al.*, 2005]. An electromagnetic wave launched on the topside of the ionosphere is unlikely to experience multiple reflections in the ionosphere and be received after each reflection, unless the wave is somehow ducted by a waveguide.

Let us now examine the possible presence and nature of waveguides. We can assume that the epsilon signatures are unlikely to be related to natural waveguides. Although in the topside Martian ionosphere, transient layers extending to hundreds of kilometers in the horizontal directions were often observed; they occurred mostly at heights below 250 km and were independent of the crustal magnetic anomalies [*Kopf et al.*, 2008; *Zhang et al.*, 2015]. Therefore, the density irregularities associated with these layers are unlikely to be responsible for the observed epsilon signatures. It is unknown whether large-scale natural plasma bubbles exist at approximately 300 km or higher, near the magnetic anomalies. Even if they exist, they cannot explain the considerably elevated apparent cutoff frequency of the epsilon signature.

On the other hand, we can assume that the sounder pulse of the MARSIS can generate appropriate field-aligned waveguides, under some conditions. The waveguide is formed by the ponderomotive force. *Morales and Lee* [1975] gave the general form of this force, whose transverse (x) and parallel (z) components are, respectively,

$$\mathbf{F}_{s,x} = -\frac{1}{8\pi}\hat{\mathbf{x}}\frac{\partial}{\partial x}\left[\left(\frac{\omega_{ps}\omega}{\omega^2 - \Omega_s^2}\right)^2 E_\perp^2 + \frac{\omega_{ps}\omega}{\omega^2 - \Omega_s^2}E_\parallel^2\right], \tag{2}$$

$$\mathbf{F}_{s,z} = -\frac{1}{8\pi}\hat{\mathbf{z}}\frac{\partial}{\partial z}\left[\left(\frac{\omega_{ps}}{\omega}\right)^2 E_\parallel^2 + \frac{\omega_{ps}^2}{\omega^2 - \Omega_s^2}E_\perp^2\right], \tag{3}$$

where s denotes the particle species (electron or ions), $\hat{\mathbf{x}}$ and $\hat{\mathbf{z}}$ are the unit vectors, and $E_{||}$ and $E_{\perp}$ are the wave electric field intensity components parallel and perpendicular to the field, respectively. The MARSIS radar transmits waves in all directions except for the dipole antenna direction. Assume that the antenna is not parallel to the magnetic field. In the near field, the wave may be approximated by a spherical wave with large gradients in $E_{||}^2$ and/or $E_{\perp}^2$, and charged particles can be driven away from the antenna by the ponderomotive force. If the particles respond to the force in an anisotropic manner (i.e., they move freely in the parallel direction but are constrained to some extent by the field lines in the perpendicular direction), then an elongated depleted region parallel to the field may form around the spacecraft. In this region, the modulational instability may occur, i.e., the wave focuses (called self-focusing) [e.g., *Gurevich et al*., 2002] or filamentation [*Boyd and Sanderson*, 2003] in the areas where the plasma density is decreased, and this focusing may in turn enhance the plasma depletion. This process may extend to the far-field region. In the far field, the gradients in $E_{||}^2$ and/or $E_{\perp}^2$ are decreased and the effect of the gradients in ω_{ps}^2 (which equals $56.4^2 N$ for electrons where N is in m^{-3} and ω_{ps} is in rad s^{-1}) becomes important. Let us consider electrons (s is removed in equation (2)) for example. For simplicity, the quantity $a = \omega/\left(\omega^2 - \Omega_e^2\right)$ is constant, and the wave is assumed to be close to a plane wave such that $E_{||} \approx 0$ (but $\partial E_{\perp}^2/\partial x \neq 0$ because of wave focusing). Equation (2) is then reduced to

$$\mathbf{F}_x \approx -\frac{a^2}{8\pi}\hat{\mathbf{x}}\left(\omega_p^2 \frac{\partial}{\partial x} E_{\perp}^2 + E_{\perp}^2 \frac{\partial}{\partial x}\omega_p^2\right). \tag{4}$$

If the transverse density gradient ($\partial\omega_p^2/\partial x$) exists, the force exerted in the direction of the density decrease is added to the otherwise axially symmetrically directed (outward from the bubble axis) ponderomotive force. As a result, the stretching bubble may be deflected to the direction of the density decrease. The deflection can increase the transverse density gradient, which in turn increases the deflection. This is consistent with the wave vector deflection by the density gradient according to equation (1). Eventually, the bubble may extend to the regions where the plasma density is low, and the wave can never be reflected. However, if $\partial\omega_p^2/\partial x = 0$ everywhere during the development of the bubble, the field-aligned bubble can continue to develop with the wave propagation, until the wave is reflected when $\omega_p = \omega$. Once formed, the bubble may persist for some time (because the magnetic field restricts the plasma motion in the perpendicular direction) and can be used by the reflected waves. How long the bubble can persist is difficult to determine; however, only several milliseconds is required, as the receiving time window of MARSIS is 7.53 ms for each transmission [*Jordan et al*., 2009].

The condition $\partial\omega_p^2/\partial x = 0$ is hard to fulfill on Mars, because a closed field line has a nearly horizontal portion, while the ionospheric density distribution has a vertical (upward decreasing) trend. This may explain the occurrence infrequency of the epsilon signatures. The condition can possibly be fulfilled to produce the epsilon signature in the regions inside a plasma cylinder but distant from the ionospheric density peak, where the transverse density gradient may be small owing to plasma trapping.

The studies of the terrestrial *F* region ionospheric modification by powerful radio emissions directed along the magnetic field lines [*Gurevich et al*., 2002] showed that when the pump wave frequency was close to the upper hybrid frequency ($f_{UH} \approx \sqrt{f_p^2 + f_{ce}^2} \approx 3$ MHz at Earth), the energy of the pump wave could be largely dissipated because of electron cyclotron resonance in strong bunched striations and plasma heating. When the pump frequency was increased to nearly thrice (9 MHz), these effects became weak and echoes of the wave could be seen. We assume that an analogous result can appear on Mars. That is, only if the sounding frequency is considerably higher than the upper hybrid frequency ($\approx f_p$ because f_{ce} is small on Mars), a waveguide can form and can be used by the pulse; otherwise, the pulse would be utilized in forming the plasma bubble and no echo will be received. This may explain why f_{OC} is 3–5 times higher than f_p (Table 1).

In addition, as Table 1 shows, the value of $f_p/|f_{ce}|$ ranges between ~100 and 1000 at the spacecraft, much larger than those (~5) seen by *Benson* [1997] on Earth. *Benson* [1997] hypothesized that the formation of a field-aligned waveguide would require this ratio to be close to an integer. Our observations suggest that this condition may not be the main, limiting requirement for the waveguide formation at Mars.

4. Conclusions

The MARSIS AIS data show a distinctive type of signal, namely, the epsilon signature, which is a combination of several oblique echo traces on the ionogram. The signature is similar in shape to that discovered previously using the ISIS radar in the terrestrial *F* region ionosphere described by *Benson* [1997]. The signature results from multiple reflections of ducted waves propagating along sounder pulse-created, field-aligned plasma bubbles (waveguides) associated with the crustal magnetic fields. The occurrence rate of the signature is low (below 0.5%) because the formation of a waveguide requires a negligible transverse (to the field lines) plasma density gradient, which is rarely met on Mars. The epsilon signatures showed cutoff frequencies 3–5 times higher than the in situ plasma frequency because the formation of waveguides requires the sounder pulse to have higher frequencies than the theoretical upper hybrid frequency. The presence of the epsilon signatures verifies the existence of the anisotropic dielectric property of the Martian ionosphere due to magnetization by the crustal magnetic anomalies at altitudes of about 300–500 km.

Acknowledgments

The MARSIS data were generated by the Italian Space Agency and NASA and published by the NASA Planetary Data System. These data are freely available through the NASA PDS Geosciences Node (http://pds-geosciences. wustl. edu/missions/). This work was funded by the Natural Science Foundation of China (projects 41274181 and 40874092). The authors are grateful to Benoit Langlais of the Laboratoire de Planétologie et Géodynamique in Nantes for providing the map of the crustal magnetic field used in producing Figure 3 of this paper.

References

Acuña, M. H., et al. (1998), Magnetic field and plasma observations at Mars: Initial results from the Mars Global Surveyor mission, *Science*, *279*, 1676–1680.

Acuña, M. H., et al. (2001), Magnetic field of Mars: Summary of results from the aerobraking and mapping orbits, *J. Geophys. Res.*, *106*(El0), 23,403–23,417, doi:10.1029/2000JE001404.

Akalin, F., D. D. Morgan, D. A. Gurnett, D. L. Kirchner, D. A. Brain, R. Modolo, M. H. Acuña, and J. R. Espley (2010), Dayside induced magnetic field in the ionosphere of Mars, *Icarus*, *206*, 104–111, doi:10.1016/j.icarus.2009.03.021.

Andrews, D. J., H. J. Opgenoorth, N. J. T. Edberg, M. André, M. Fränz, E. Dubinin, F. Duru, D. Morgan, and O. Witasse (2013), Determination of local plasma densities with the MARSIS radar: Asymmetries in the high-altitude Martian ionosphere, *J. Geophys. Res. Space Physics*, *118*, 1–15, doi:10.1002/jgra.50593.

Andrews, D. J., M. Andre, H. J. Opgenoorth, N. J. T. Edberg, C. Dieval, F. Duru, D. A. Gurnett, D. Morgan, and O. Witasse (2014), Oblique reflections in the Mars Express MARSIS data set: Stable density structures in the Martian ionosphere, *J. Geophys. Res. Space Physics*, *119*, 3944–3960, doi:10.1002/2013JA019697.

Andrews, D. J., N. J. T. Edberg, A. I. Eriksson, D. A. Gurnett, D. Morgan, F. Němec, and H. J. Opgenoorth (2015), Control of the topside Martian ionosphere by crustal magnetic fields, *J. Geophys. Res. Space Physics*, *120*, 3042–3058, doi:10.1002/2014JA020703.

Beharrell, M. J., and J. A. Wild (2012), Stationary flux ropes at the southern terminator of Mars, *J. Geophys. Res.*, *117*, A12212, doi:10.1029/2012JA017738.

Benson, R. F. (1997), Evidence for the stimulation of field-aligned electron density irregularities on a short time scale by ionospheric topside sounders, *J. Atmos. Sol. Terr. Phys.*, *59*(18), 2281–2293.

Boyd, T. J. M., and J. J. Sanderson (2003), *The Physics of Plasmas*, pp. 197–245, Cambridge Univ. Press, New York.

Brain, D. A., R. J. Lillis, D. L. Mitchell, J. S. Halekas, and R. P. Lin (2007), Electron pitch angle distributions as indicators of magnetic field topology near Mars, *J. Geophys. Res.*, *112*, A09201, doi:10.1029/2007JA012435.

Calvert, W. (1995), Wave ducting in different wave modes, *J. Geophys. Res.*, *100*, 17,491–17,497, doi:10.1029/95JA01131.

Diéval, C., D. J. Andrews, D. D. Morgan, D. A. Brain, and D. A. Gurnett (2015), MARSIS remote sounding of localized density structures in the dayside Martian ionosphere: A study of controlling parameters, *J. Geophys. Res. Space Physics*, *120*, 8125–8145, doi:10.1002/2015JA021486.

Duru, F., D. A. Gurnett, T. F. Averkamp, D. L. Kirchner, R. L. Huff, A. M. Persoon, J. J. Plaut, and G. Picardi (2006), Magnetically controlled structures in the ionosphere of Mars, *J. Geophys. Res.*, *111*, A12204, doi:10.1029/2006JA011975.

Duru, F., D. A. Gurnett, D. D. Morgan, R. Modolo, A. F. Nagy, and D. Najib (2008), Electron densities in the upper ionosphere of Mars from the excitation of electron plasma oscillations, *J. Geophys. Res.*, *113*, A07302, doi:10.1029/2008JA013073.

Duru, F., D. D. Morgan, and D. A. Gurnett (2010), Overlapping ionospheric and surface echoes observed by the Mars Express radar sounder near the Martian terminator, *Geophys. Res. Lett.*, *37*, L23102, doi:10.1029/2010GL045859.

Dyson, P. L., and R. F. Benson (1978), Topside sounder observations of equatorial bubbles, *Geophys. Res. Lett.*, *5*, 795–798, doi:10.1029/GL005i009p00795.

Fitzpatrick, R. (2008), *Plasma Physics*, The Univ. Texas, Austin. [Available at http://farside.ph.utexas.edu/teaching/plasma/Plasma/index.html.]

Fox, J. L., and K. E. Yeager (2006), Morphology of the near-terminator Martian ionosphere: A comparison of models and data, *J. Geophys. Res.*, *111*, A10309, doi:10.1029/2006JA011697.

Gurevich, A. V., K. P. Zybin, H. C. Carlson, and T. Pedersen (2002), Magnetic zenith effect in ionospheric modifications, *Phys. Lett. A*, *305*, 264–274.

Gurnett, D. A., et al. (2005), Radar soundings of the ionosphere of Mars, *Science*, *310*, 1929–1933, doi:10.1126/science.1121868.

Gurnett, D. A., et al. (2008), An overview of radar soundings of the Martian ionosphere from the Mars Express spacecraft, *Adv. Space Res.*, *41*, 1335–1346, doi:10.1016/j.asr.2007.01.062.

Gurnett, D. A., D. D. Morgan, F. Duru, F. Akalin, J. D. Winningham, R. A. Frahm, E. Dubinin, and S. Barabash (2010), Large density fluctuations in the Martian ionosphere as observed by the Mars express radar sounder, *Icarus*, *206*(1), 83–94, doi:10.1016/j.icarus.2009.02.019.

Jordan, R., et al. (2009), The Mars express MARSIS sounder instrument, *Planet. Space Sci.*, *57*, 1975–1986, doi:10.1016/j.pss.2009.09.016.

Kopf, A. J., D. A. Gurnett, D. D. Morgan, and D. L. Kirchner (2008), Transient layers in the topside ionosphere of Mars, *Geophys. Res. Lett.*, *35*, L17102, doi:10.1029/2008GL034948.

Krymskii, A. M., T. K. Breus, N. F. Ness, M. H. Acuña, J. E. P. Connerney, D. H. Crider, D. L. Mitchell, and S. J. Bauer (2002), Structure of the magnetic field fluxes connected with crustal magnetization and topside ionosphere at Mars, *J. Geophys. Res.*, *107*(A9), 1245, doi:10.1029/2001JA000239.

Langlais, B., M. E. Purucker, and M. Mandea (2004), Crustal magnetic field of Mars, *J. Geophys. Res.*, *109*, E02008, doi:10.1029/2003JE002048.

Lillis, R. J., H. V. Frey, M. Manga, D. L. Mitchell, R. P. Lin, M. H. Acuña, and S. W. Bougher (2008), An improved crustal magnetic field map of Mars from electron reflectometry: Highland volcano magmatic history and the end of the Martian dynamo, *Icarus*, *194*, 575–596, doi:10.1016/j.icarus.2007.09.032.

Mitchell, D. L., R. P. Lin, C. Mazelle, H. Rème, P. A. Cloutier, J. E. P. Connerney, M. H. Acuña, and N. F. Ness (2001), Probing Mars' crustal magnetic field and ionosphere with the MGS Electron Reflectometer, *J. Geophys. Res.*, *106*(El0), 23,419–23,427, doi:10.1029/2000JE001435.

Morales, G. J., and Y. C. Lee (1975), Nonlinear filamentation of lower-hybrid cones, *Phys. Rev. Lett.*, *35*(14), 930–933.

Morgan, D. D., D. A. Gurnett, D. L. Kirchner, J. L. Fox, E. Nielsen, and J. J. Plaut (2008), Variation of the Martian ionospheric electron density from Mars Express radar soundings, *J. Geophys. Res.*, *113*, A09303, doi:10.1029/2008JA013313.

Morgan, D. D., D. A. Gurnett, F. Akalin, D. A. Brain, J. S. Leisner, F. Duru, R. A. Frahm, and J. D. Winningham (2011), Dual-spacecraft observation of large-scale magnetic flux ropes in the Martian ionosphere, *J. Geophys. Res.*, *116*, A02319, doi:10.1029/2010JA016134.

Morgan, D. D., O. Witasse, E. Nielsen, D. A. Gurnett, F. Duru, and D. L. Kirchner (2013), The processing of electron density profiles from the Mars Express MARSIS topside sounder, *Radio Sci.*, *48*, 197–207, doi:10.1002/rds.20023.

Němec, F., D. D. Morgan, D. A. Gurnett, F. Duru, and V. Truhlík (2011), Dayside ionosphere of Mars: Empirical model based on data from the MARSIS instrument, *J. Geophys. Res.*, *116*, E07003, doi:10.1029/2010JE003789.

Ness, N. F., M. H. Acuña, J. E. P. Connerney, A. J. Kliore, T. K. Breus, A. M. Krymskii, P. Cloutier, and S. J. Bauer (2000), Effects of magnetic anomalies discovered at Mars on the structure of the Martian ionosphere and solar wind interaction as follows from radio occultation experiments, *J. Geophys. Res.*, *105*, 15,991–16,004, doi:10.1029/1999JA000212.

Nielsen, E., H. Zou, D. A. Gurnett, D. L. Kirchner, D. D. Morgan, R. Huff, R. Orosei, A. Safaeinili, J. J. Plaut, and G. Picardi (2006), Observations of vertical reflections from the topside Martian ionosphere, *Space Sci. Rev.*, *126*, 373–388, doi:10.1007/s11214-006-9113-y.

Nielsen, E., X. D. Wang, D. A. Gurnett, D. L. Kirchner, R. Huff, R. Orosei, A. Safaeinili, J. J. Plaut, and G. Picardi (2007), Vertical sheets of dense plasma in the topside Martian ionosphere, *J. Geophys. Res.*, *112*, E02003, doi:10.1029/2006JE002723.

Picardi, G., et al. (2004), MARSIS: Mars advanced radar for subsurface and ionosphere sounding, in *Mars Express: A European Mission to The Red Planet, SP-1240*, edited by A. Wilson, pp. 51–70, European Space Agency Publication Division, Noordwijk, Netherlands.

Wang, X.-D., J.-S. Wang, E. Nielsen, and H. Zou (2009), "Hook" structure in MARSIS ionogram and its interpretation, *Geophys. Res. Lett.*, *36*, L13103, doi:10.1029/2009GL038844.

Wang, X.-D., J.-S. Wang, and H. Zou (2012), On the small-scale fluctuations in the peak electron density of Martian ionosphere observed by MEX/MARSIS, *Planet. Space Sci.*, *63–64*, 87–93, doi:10.1016/j.pss.2011.10.007.

Withers, P. (2009), A review of observed variability in the dayside ionosphere of Mars, *Adv. Space Res.*, *44*, 277–307, doi:10.1016/j.asr.2009.04.027.

Zhang, Z., R. Orosei, Q. Huang, and J. Zhang (2015), Topside of the Martian ionosphere near the terminator: Variations with season and solar zenith angle and implications for the origin of the transient layers, *Icarus*, *251*, 12–25, doi:10.1016/j.icarus.2014.09.036.